Ultrafast Excited State Dynamics of the Protonated Schiff Base of All-*trans* Retinal in Solvents

Goran Zgrablić,* Kislon Voïtchovsky,* Maik Kindermann,† Stefan Haacke,* and Majed Chergui*
*Laboratoire de Spectroscopie Ultrarapide and †Laboratory of Protein Engineering, Ecole Polytechnique Fédérale de Lausanne, Institute of Chemical Sciences and Engineering, FSB-BSP, CH-1015 Lausanne-Dorigny, Switzerland

ABSTRACT We present a comparative study of the ultrafast photophysics of all-*trans* retinal in the protonated Schiff base form in solvents with different polarities and viscosities. Steady-state spectra of retinal in the protonated Schiff base form show large absorption-emission Stokes shifts (6500–8100 cm^{-1}) for both polar and nonpolar solvents. Using a broadband fluorescence up-conversion experiment, the relaxation kinetics of fluorescence is investigated with 120 fs time resolution. The time-zero spectra already exhibit a Stokes-shift of ~6000 cm^{-1}, indicating depopulation of the Franck-Condon region in ≤100 fs. We attribute it to relaxation along skeletal stretching. A dramatic spectral narrowing is observed on a 150 fs timescale, which we assign to relaxation from the S_2 to the S_1 state. Along with the direct excitation of S_1, this relaxation populates different quasistationary states in S_1, as suggested from the existence of three distinct fluorescence decay times with different decay associated spectra. A 0.5–0.65 ps decay component is observed, which may reflect the direct repopulation of the ground state, in line with the small isomerization yield in solvents. Two longer decay components are observed and are attributed to torsional motion leading to photo-isomerization. The various decay channels show little or no dependence with respect to the viscosity or dielectric constant of the solvents. This suggests that in the protein, the bond selectivity of isomerization is mainly governed by steric effects.

INTRODUCTION

All-*trans* retinal is the photosensitive chromophore in many bacterial forms of retinal proteins such as bacteriorhodopsin and sensory rhodopsin II found in *Halobacterium salinarum* (Oesterhelt and Stoeckenius, 1971). These relatively small proteins are important model systems for transmembrane proton/ion pumping and for bacterial photosensors involved in phototaxis. As a general feature conserved in all retinal proteins, retinal is covalently bound to the nitrogen atom of a lysine residue leading to the protonated Schiff base form of retinal (PSBR). Ultrafast photo-isomerization is an important premise of the protein function and has thus been characterized extensively by femtosecond (fs) pump-probe and fluorescence spectroscopy in retinal proteins (Dexheimer et al., 1992; Dobler et al., 1988; Du and Fleming, 1993; Mathies et al., 1988; Polland et al., 1986; Schoenlein et al., 1991; Sharkov et al., 1985; Wang et al., 1994). Very recently, fs midinfrared spectroscopy has confirmed the *trans-cis* isomerization in the protein to occur in 450–500 fs (Herbst et al., 2002). Ultrafast (<50 fs) structural relaxation of excited retinal, most probably along C=C stretching modes, has also been revealed by fs-visible spectroscopy (Song and El-Sayed, 1998; Ye et al., 1999), also at very high time resolution (Kobayashi et al., 2001). This is a direct consequence of the bond order change in the excited state (González-Luque et al., 2000), required for the isomerization to occur.

Besides the intraretinal dynamics, the exact role of the protein environment is still not understood at a microscopic level. Indeed in bacteriorhodopsin (bR), the isomerization yield of retinal is high (65%) and occurs selectively around the C_{13}=C_{14} double bond, whereas in solution the yield is low (<20%) and the isomerization is highly nonselective (Becker and Freedman, 1985; Koyama et al., 1991). It was suggested that this ''catalytic'' action of the protein is determined by the presence of charged residues (Arg^{82}, Asp^{85}, Asp^{212}) in the vicinity of retinal (Heyne et al., 2000; Nonella, 2000; Song et al., 1993). Furthermore, PSBR undergoes a 12–18 D dipole moment change upon vertical excitation (Mathies and Stryer, 1976; Ponder and Mathies, 1983; Huang et al., 1989), and it has been suggested that the sudden polarization of the protein pocket induces an ultrafast dielectric response of the environment (Kennis et al., 2002; Xu et al., 1996), similar to those found in polar solvents (Maroncelli and Fleming, 1988), which may also drive the isomerization dynamics.

To address this issue, it is useful to investigate the ultrafast photophysics of the retinylidene chromophore as a function of solvent properties, such as viscosity and dielectric constant. This would help disentangle intramolecular dynamics (internal conversion, isomerization) from the intermolecular ones (dielectric response, viscosity) and clarify the interplay between the two, bearing in mind the low yield and unselective isomerization in solutions (Freedman and Becker, 1986; Koyama et al., 1991). Absorption and fluorescence

Submitted May 17, 2004, and accepted for publication January 11, 2005.

Address reprint requests to Stefan Haacke, E-mail: stefan.haacke@ipcms.u-strasbg.fr.

Maik Kindermann's new address is COVALYS Biosciences AG, CH-4108 Witterswil, Switzerland.

Stefan Haacke's new address is Institut de Physique et Chimie des Matériaux de Strasbourg-GONLO, 23 rue du Loess, F-67034 Strasbourg Cédex, France.

0006-3495/05/04/2779/10 $2.00

doi: 10.1529/biophysj.104.046094

studies of unprotonated and protonated *n*-butylamine Schiff bases of all-*trans* retinal were performed (Becker and Freedman, 1985; Freedman and Becker, 1986), along with measurements of the fluorescence quantum yields and lifetimes (Bachilo et al., 1996; Bachilo and Gillbro, 1999; Huppert and Rentzepis, 1986). From these studies, it was concluded (Bachilo et al., 1996) that both absorption and emission of the PSBR forms are dominated by the same $S_0 - S_1$ transition with strong one-photon allowed ^1A_g-^1B_u character.

The ultrafast spectroscopy of all-*trans* PSBR in solution has been reported by a few groups (Hamm et al., 1996; Kandori and Sasabe, 1993; Logunov et al., 1996). In fluorescence up-conversion, an initial 100 fs decay was observed, followed by a slower 3–7 ps decay time of the excited state. Although initially these decay times were attributed to isomerization, more recent work carried out on 13-*cis* locked retinal analogs, which revealed similarly short decay times, put this interpretation in question (Hou et al., 2001). In addition, since the *cis* and *trans* isomers in solution have very similar absorption spectra, it has not been possible to give direct evidence for the formation of the *cis* forms. Finally, a systematic solvent dependence study of PSBR dynamics in solution has not been carried out.

Here we report on the ultrafast spectral evolution of the fluorescence of all-*trans* PSBRs in protic (methanol MeOH, 1-octanol OctOH, and 2-propanol ProOH) and nonprotic (cyclohexane cHex and dichloromethane DCM) solvents. The rationale behind this choice is that they differ by more than one order of magnitude in viscosity and dielectric constants (Table 1). These physical parameters are known to strongly affect the intramolecular structural response and the intermolecular dielectric response of molecules in solvents (Horng et al., 1995). For example, OctOH shows a relatively slow dielectric relaxation time of 27 ps, whereas MeOH has an average relaxation time of 3–5 ps (Horng et al., 1995).

Using the fluorescence up-conversion technique in a ''polychromatic mode'' (Haacke et al., 1998), we are able to monitor excited state relaxation in a very detailed fashion through the rise, decay, and shifts of the time-gated emission spectra. We identify two emission bands, a short lived, high-energy band, which we attribute to emission from S_2, and a longer lived, low-energy one that decays in a multiexponential fashion. The short component (550 ± 50 fs) of the latter represents return to the all-*trans* ground state, and the picosecond-long ones to isomerization around various carbon bonds. The decay constants show little or no dependence on viscosity and dielectric constant. These results point to intramolecular processes as the main actors in the ultrafast dynamics of PSBR in solution.

EXPERIMENTAL PROCEDURES

The fluorescence up-conversion experiment is based on a Ti:Sapphire laser system with a 250 kHz regenerative amplifier (Coherent RegA-9050/Mira Seed; Coherent, Santa Clara, CA) delivering 40–50 fs pulses at 850 nm. The excitation beam was generated by frequency doubling in a 500 μm-thick BBO crystal. The *n*-butylamine Schiff bases of all-*trans* retinal were prepared according to previously described methods (Hamm et al., 1996) and protonated using a 3–5-fold excess of trichloracetic acid. Anhydrous solvents (Fluka, Buchs, Switzerland, or VWR, Dietikon, Switzerland) were

TABLE 1 Solvent properties and results of the data analysis of all-*trans* PSBR in solution

Solvent	MeOH	ProOH	OctOH	DCM	cHex
ε ($\omega = 0$)	32.66	20.45	9.80	8.93	2.02
n_d	1.327	1.384	1.4295	1.421	1.424
η (mPa s)	0.547	1.96	7.4	0.401	1.0
ΔE_{Stokes} (cm^{-1})	8100	-	6950	-	6550
FWHM (cm^{-1})	3900	-	4850	-	5300
Band I					
$\tau_{I,1}$/ps	0.64 (0.35)	0.64 (0.42)	0.50 (0.45)	0.63 (0.46)	0.56 (0.48)
$\tau_{I,2}$/ps	1.5 (0.30)	2.2 (0.37)	2.5 (0.36)	2.0 (0.32)	2.1 (0.40)
$\tau_{I,3}$/ps	4.6 (0.35)	5.5 (0.21)	6.3 (0.19)	4.7 (0.22)	3.7 (0.12)
$\langle\tau\rangle$ /ps	2.3	2.2	2.3	2.0	1.55
$\lambda_{I,1}$/nm	610	600	620	605	605
$\lambda_{I,2}$/nm	610	623	620	643	640
$\lambda_{I,3}$/nm	660	650	620	660	620
$w_{I,1}$/nm	100	110	140	90	140
$w_{I,2}$/nm	100	120	140	110	120
$w_{I,3}$/nm	75	90	140	80	150
Band II					
$\tau_{II,1}$/fs	<30 (0.76)	<30 (0.87)	<30 (0.89)	<30 (0.85)	<30 (0.88)
$\tau_{II,2}$/fs	170 (0.24)	140 (0.13)	150 (0.11)	140 (0.15)	150 (0.12)
λ_{II}/nm	544	537	523	550	517
w_{II}/nm	90	90	85	95	95

Static dielectric constant ε ($\omega = 0$), refractive index n_d, and absolute viscosity η (all at 25°C, taken from Riddick et al., 1986). Peak-to-peak Stokes shift ΔE_{Stokes} and FWHM of the time-integrated fluorescence. Decay times τ_i, relative amplitudes a_i (in parentheses), central wavelengths λ, and FWHMs w of the DAS of bands I and II in different solvents. $\langle\tau\rangle$ is the average decay time of band I, defined in the text. Lifetimes are given with the following uncertainties: $\tau_{I,1}$, $\pm$ 0.08 ps; $\tau_{I,2}$, $\pm$ 0.3 ps; $\tau_{I,3}$, $\pm$ 0.5 ps; $\tau_{II,1}$, $\pm$ 15 fs; and $\tau_{II,1}$, $\pm$ 20 fs.

used as received; ~250 mL of the PSBR solution (optical density 9–15/cm) is flown through a 0.3 mm path length flow cell using a dye laser pump (flow speed 5–6 m/s), and the fluorescence is collected in transmission geometry. For excitation, 20 nJ pulses were focused in a spot of ~40 μm diameter (~1.4 mJ/cm^2). Thus, ~20% of the molecules are excited per shot in the focal volume. In contrast with our previously published data (Zgrablić et al., 2004), the sample circulation speed was better matched with the high laser repetition rate and the sample volume contains <10% *cis* isomers. Accumulation of *cis* isomers after 4–5 h of exposure slightly changes the kinetics (disappearance of two-band signatures and oscillatory features), but the data reported here have been obtained on freshly prepared samples that were exposed not more than 60 min.

A BBO crystal of 250 μm thickness is used for the sum frequency generation. We work in a ''polychromatic'' mode, where by turning the up-conversion crystal, the whole spectral region of interest is phase matched, removing the limit of the intrinsic crystal's acceptance bandwidth (Haacke et al., 1998). Throughout the rotation, the up-converted fluorescence is continuously acquired with a spectrometer and a LN_2-cooled, back-illuminated charge-coupled device camera (15 s exposure time). After the up-conversion crystal, the sum frequency beam goes through a pinhole followed by a combination of a quartz prism and a mask, which filter unwanted long-wavelength light: the 850 nm gate beam, non-up-converted fluorescence, and more importantly the second harmonic of the fundamental. An additional Schott UG11 UV pass filter (Schott Glass Technologies, Mainz, Germany) reduces this signal further but limits the spectral window to $\lambda < 720$ nm. The remaining background signal, measured at negative delay times, is averaged and subtracted from the raw data. Time-resolved spectra are not corrected for the spectral sensitivity of the detection system.

The group velocity dispersion induced by optical elements in the fluorescence path (including a GG420 filter) was measured using white light generated by 800-nm pulses in the same flow cell filled with water. By observing the up-converted Raman line of the solvent, time zero was determined, along with the instrument time response function of 120–150 fs width. The spectral resolution of the instrument is equivalent to 14 nm in the fluorescence spectrum determined by up-converting a He-Ne laser line.

Steady-state spectra are recorded in a PerkinElmer (Wellesley, MA) spectrophotometer and in a modified Spex (Edison, NJ) fluorimeter. The latter is equipped with a Si avalanche diode for recording the near-IR fluorescence with higher efficiency. The data $I(\lambda)d\lambda$ are corrected for the instrument response, determined by using standard red-emitting dyes (pyridine 2, oxazine 750, and styryl 11), and multiplied by λ^2 upon conversion from wavelengths to wavenumbers (Lakowicz, 1999). The steady-state fluorescence spectra are obtained on samples with optical density 0.5–0.6/cm under excitation at 450 nm.

RESULTS

In the following, we mainly present results concerning the most and least polar solvents: MeOH and cHex, whereas Table 1 and Fig. 8 compile the results with all solvents studied here.

Steady-state spectra

The steady-state absorption and fluorescence spectra of the PSBRs in different solvents exhibit interesting differences as a function of solvent polarity (Fig. 1). As reported previously (Bachilo et al., 1996), the absorption shifts slightly to the red for hydrogen-bonding solvents with increasing polarizability (refractive index n in Table 1), but the absorption spectra show only small bathochromic shifts. The absorption maxima lie within 21,700–22,700 cm^{-1}, and the spectral

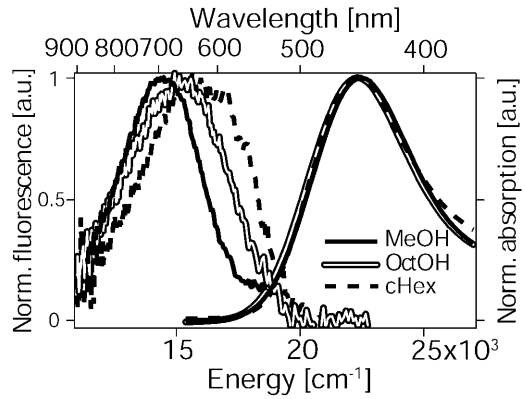

FIGURE 1 Steady-state absorption and fluorescence spectra of PSBR obtained in methanol, octanol, and cyclohexane. The fluorescence spectra are corrected for background signals and the fluorimeter instrument response function.

width does not change significantly as a function of solvent properties. We find a full width at half-maximum (FWHM) of ~5200 cm^{-1}, which is ~30% larger than for all-*trans* PSBR in retinal proteins. It is well possible that the S_0–S_2 transition contributes to the absorption profile but is unresolved. It may have nonnegligible one-photon character, as in the case of bR (Birge and Zhang, 1990). Due to the trichloracetic acid counterion, the S_1–S_2 separation is expected to be considerably smaller in the solvents than the value of 5000 cm^{-1} obtained by calculations for the isolated chromophore (De Vico et al., 2002). For $E > 28{,}000$ cm^{-1}, the absorption spectrum shows contributions of nonprotonated Schiff bases (Freedman and Becker, 1986).

A somewhat more pronounced solvent dependence is observed in the fluorescence spectra. PSBRs in MeOH has the red-most spectrum and a ~30% smaller spectral width than the chromophores in OctOH and cHex (cf. Table 1). One has to keep in mind that the steady-state spectra are an average over a short fluorescence lifetime: 2.3 ps for MeOH and OctOH, and ~1.6 ps for cHex (see $\langle\tau\rangle$ in Table 1). For OctOH, the fluorescence lifetime is much shorter than the dielectric relaxation time (Horng et al., 1995), whereas the nonpolar cHex is known to show no dielectric Stokes shift at all (Reynolds et al., 1996). On the other hand, since MeOH is the most polar solvent with the fastest solvation dynamics among the alcohols studied here (Horng et al., 1995), a red-shift is expected as a consequence of dielectric solvation. The peak-to-peak Stokes shift decreases with decreasing dielectric constant (Table 1). As cHex is nonpolar, the PSBR/cHex Stokes shift of 6550 cm^{-1} is dominated by intramolecular relaxation. The difference with respect to MeOH (~1600 cm^{-1}), which amount to ~20% of the total Stokes shift for that solvent, should reflect the intermolecular contributions (dielectric solvation, hydrogen-bonding, inhomogeneous broadening, etc.). The latter are also hinted at by the larger widths of the fluorescence spectra in OctOH and cHex.

Time-resolved fluorescence spectra

Fig. 2, *A* and *B*, displays two-dimensional contour plots of PSBR emission in MeOH and cHex. In the initial phase, i.e., from negative delays until $t = 200$ fs, the spectra are extremely broad, extending from 500 to 700 nm (FWHM = 6000 cm^{-1}). They are already considerably red-shifted with respect to the corresponding absorption maximum. The high-energy part decays quite dramatically with time, leading to a reduction of the spectral width of ~1500 cm^{-1} by $t = 100$ fs (Fig. 3, *A* and *C*). The fact that already at negative times, the spectrum spans nearly the whole energy range of the steady-state Stokes shift suggests an extremely fast initial relaxation process taking place on a timescale much shorter than our time resolution of ≈120 fs.

In a second slower stage (Fig. 3, *B* and *D*), the spectra narrow down significantly for PSBR/MeOH (FWHM = 2080 cm^{-1} at 4 ps), whereas they remain fairly broad for PSBR/cHex (FWHM = 3150 cm^{-1} at 4 ps) and other less polar solvents. In MeOH, the spectral narrowing is accompanied by a dynamic red-shift of the spectrum. The latter is not larger than 300 cm^{-1} (shift of maximum) from $t = 0$–6.0 ps but may not be entirely captured for the longest delay times, due to the cutoff of the UG11 filter. In cHex on the other hand, no dynamic red-shift is visible even for the longest delay times. As this data set does not fully show the low-energy part of the emission, we will not address these slower components of dielectric relaxation in the following.

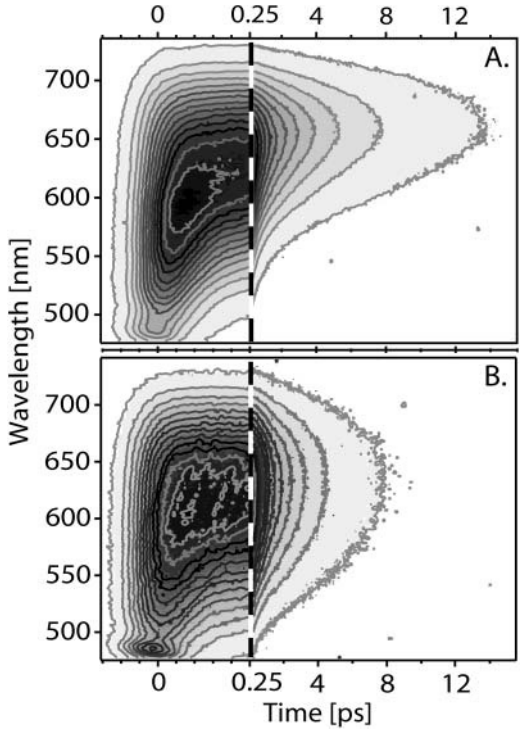

FIGURE 2 Two-dimensional contour plots of the time-resolved fluorescence spectra of all-*trans* PSBR in MeOH (*A*) and cHex (*B*). The data in panel *B* were normalized to the maximum intensity of the fluorescence in panel *A*. The contour lines appear with steps of 7% of the maximum intensity. The first 0.25 ps are enlarged to emphasize the rise region. Note the Raman peak of the solvent appearing at 490 nm, particularly in cHex.

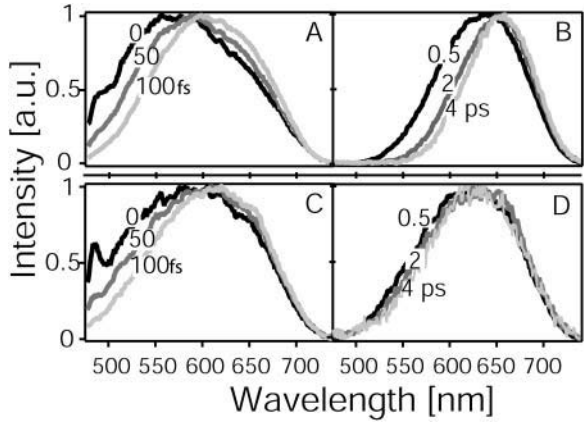

FIGURE 3 Normalized fluorescence spectra of the PSBR in MeOH (*A* and *B*) and cHex (*C* and *D*) at different delay times.

Kinetic traces

The fluorescence decay is almost complete within 15 ps, in agreement with an excited state lifetime of 4–6 ps (Hamm et al., 1996; Logunov et al., 1996; Kandori and Sasabe, 1993). Fig. 4 shows four kinetic traces for PSBR/MeOH at characteristic wavelengths. At the high-energy side (485–550 nm), after an instantaneous rise, ~80% of the fluorescence decays on a sub-50 fs timescale, as indicated by the slight asymmetry of the 530-nm trace, whereas the remaining part decays with a time constant of $\tau_{II,2} = 150 \pm 20$ fs, as suggested by the spectral kinetics described above and reported earlier (Kandori and Sasabe, 1993).

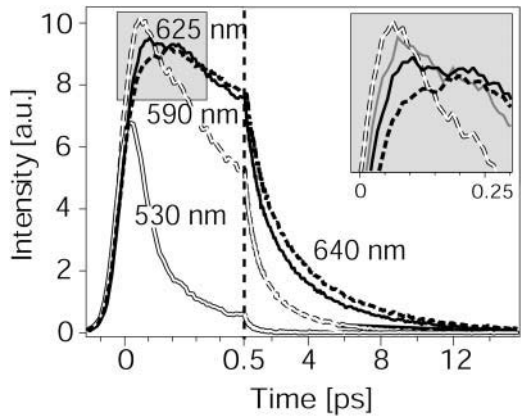

FIGURE 4 Fluorescence decay curves of all-*trans* PSBR in MeOH at 530 nm (*double line*), 590 nm (*double dashed line*), 625 nm (*solid line*), and 640 nm (*dashed line*). The first 0.5 ps are enlarged. (*Inset*) Region of maximum intensity between 0 and 0.3 ps (*shaded area*) with an additional trace at 610 nm (*light gray*).

For $\lambda = 640$–740 nm, the time-zero spectra of Fig. 3, *A* and *C*, show that part of the signal rises within the experimental time resolution, followed by a slower rising component. For the total signal build-up, we fit a wavelength-independent rise time $\tau_{I,r} = 130 \pm 30$ fs, which, to our knowledge, was not reported previously (Kandori and Sasabe, 1993). This value correlates well with the $\tau_{II,2} = 150$ fs decay observed at shorter wavelengths. Note that the dynamic red-shift observed for PSBR/MeOH (cf. Fig. 3 *B*) occurs on a slower timescale and does not contribute to the sub-200 fs rise times discussed here.

For intermediate wavelengths (550–640 nm), we observe an abrupt change in the behavior of the rise time. Indeed, the fluorescence rises instantaneously from the blue edge up to 600 nm. Then from 600 nm on, the above 130 fs rise component appears and is observed up to the red-most edge. This behavior is best seen from the tilt of the contour lines for $\lambda >$ 600 nm in Fig. 2. In the case of a sequential relaxation mechanism on the same electronic surface, we would expect a gradual increase of the rise time, in going from the high- to the low-energy fluorescence. However, the abrupt change of the rise time over <50 nm suggests the existence of two distinct overlapping bands: a low-energy slowly rising/decaying one (band I $\lambda > 550$ nm), and a high-energy fast-rising/decaying one (band II $\lambda < 640$ nm). At intermediate wavelengths, the signal is a linear combination of both bands. The shape of the trace at 625 nm corroborates this finding: an almost constant signal level is observed between 100 and 300 fs (Fig. 4). This plateau is due to the two bands contributing with nearly similar amplitudes. Going from 625 nm to longer wavelengths, the high-energy band II gradually loses intensity, making it possible to observe the slow rise of the low-energy band. On the other hand, going to the shorter wavelengths ($\lambda < 625$ nm) the high-energy band dominates, masking the rise of the low-energy band I (Fig. 4, *inset*). A more elaborate singular value decomposition (SVD) analysis allows separating the two emission bands (see below).

When the rise is finally completed, the later part of the kinetic traces reveals a complex decay of the low-energy band in every measured solvent. Fig. 5 compares residuals of bi- and triexponential fits to the MeOH data. They demonstrate—alongside a threefold reduction of the χ^2 values—that the decays are triexponential around 600 nm. The decay constants and preexponential factors are listed in Table 1 for all solvents studied here.

Decay associated spectra

To disentangle bands I and II, we note that in Fig. 2, the fluorescence for $\lambda > 640$ nm is due to the band I only. Thus, the SVD applied to this red-most part will determine exclusively the rise and decay constants of band I, but the extracted decay associated spectra (DAS) are not complete since the wavelengths below 640 nm are missing. When applying the SVD over the whole wavelength range but only

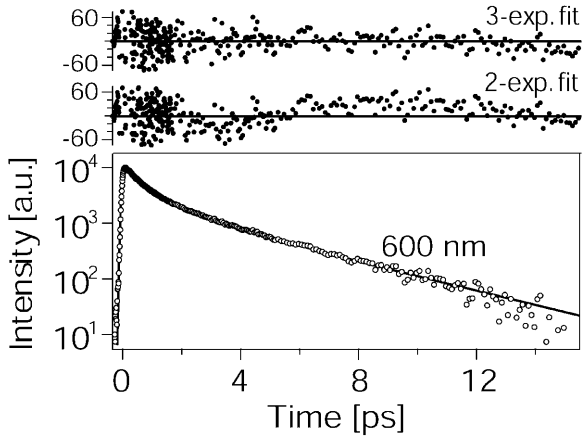

FIGURE 5 (*Lower panel*) Triexponential fit (*solid line*) of the fluorescence time trace at 600 nm (*open circles*) of PSBR/MeOH in a semi-logarithmic plot. (*Top panel*) Residuals for tri- and biexponential fits.

from $t = 300$ fs (when the rise is over and the contribution of the Band II is negligible, Fig. 3), the information about the time evolution for earlier times is lost, but we recover the full DAS of band I. With the principal time constants and the DAS, we reconstruct a noise-free band I* for the entire time and wavelength range. Subsequently subtracting band I* from the original fluorescence, we recover band II. This approach is not intrinsically suitable for bands that evolve spectrally, but the time-resolved spectra show that spectral evolution occurs at the shortest times, and is negligible at later ones, even in the most polar solvent (MeOH). The DAS for MeOH and cHex are shown in Figs. 6 *A* and 7 *A*, respectively, and the parameters for all solvents are given in Table 1. Figs. 6 *B* and 7 *B* show the kinetic traces at the central wavelengths of bands I and II. Fig. 8 shows the spectral decomposition into bands I and II for the solvents studied here, where each spectrum was taken at the moment

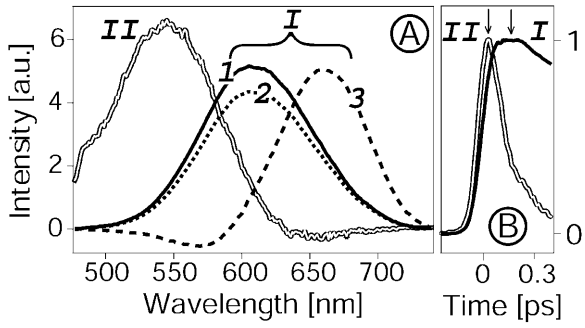

FIGURE 6 (*A*) DAS of the all-*trans* PSBR fluorescence in MeOH. Band I is composed of three DAS, I1, I2, and I3, determined using the SVD analysis (see text and Table 1 for parameters). Spectrum II shows the maximum intensity of the band II ($t = 0$ fs). (*B*) Time traces I and II taken at the central wavelengths of band I (640 nm) and band II (540 nm), respectively. A biexponential fit on the trace II gives $\tau_{II,1} = (20 \pm 10)$ fs (76%) and $\tau_{II,2} = (170 \pm 20)$ fs (24%).

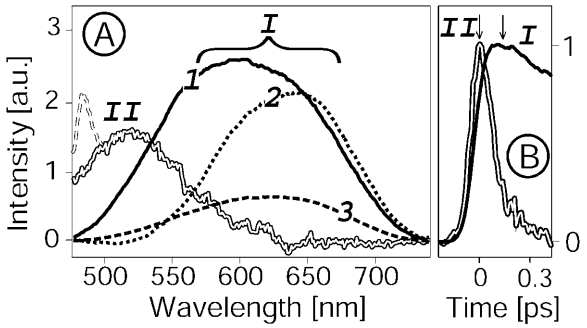

FIGURE 7 (*A*) DAS of the all-*trans* PSBR fluorescence in cHex. Annotations as for Fig. 6. The double-dashed line plots the Raman peak, subtracted from band II. (*B*) Time traces taken at the central wavelengths of band I and II, respectively. Trace II is best fitted with $\tau_{II,1} = (20 \pm 10)$ fs (88%) and $\tau_{II,2} = (150 \pm 20)$ fs (12%).

of maximum intensity of the band (*arrows* in Figs. 6 *B* and 7 *B*). We note the following:

Band II

More than 80% of the fluorescence rises and decays with the excitation pulse, the rest decays in ≈150 fs (trace II Figs. 6 *B* and 7 *B*, Table 1).The band maximum shows a red-shift with increasing dielectric constant (Fig. 8) within each class of solvents, whereas the FWHM remains fairly constant around 90 nm. Nevertheless, the timescales associated with band II are nearly identical for the whole series of solvents, and the preexponential factors differ slightly, but with no apparent systematic trend as a function of dielectric constant and/or viscosity.

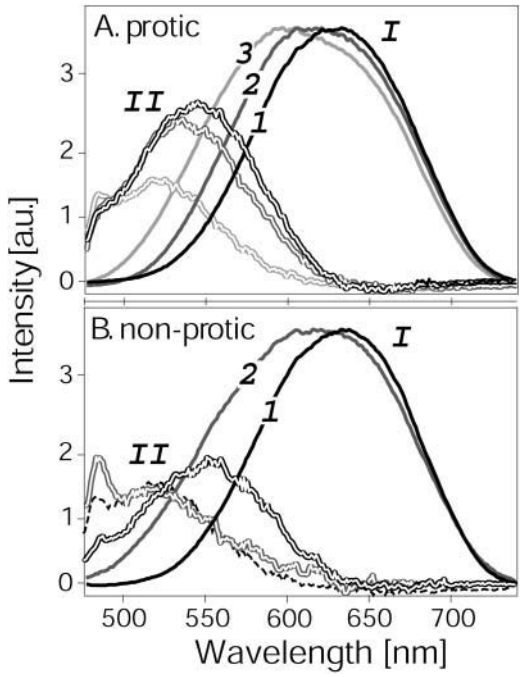

FIGURE 8 Relative intensities of band I and II in different solvents. (*A*) Protic: methanol, 1; propanol, 2; and octanol, 3. Bands I and II, belonging to the same solvent, have the same gray shade coding. (*B*) Nonprotic: dichloromethane, 1, and cyclohexane, 2. For the sake of comparison, the dashed line plots band II for octanol. For every solvent, the spectra of band I (*solid line*) and of band II (*double line*) are taken at the time when the band reaches its maximum intensity (see *arrows* in Figs. 6 *B* and 7 *B*). For each solvent, the pair of spectra were normalized to the maximum intensity of band I in methanol.

Band I

In this case, we extracted three DAS with distinct timescales: a fast one $\tau_{I,1} = 0.5$–0.64 ps, an intermediate one $\tau_{I,2} = 1.5$–2.5 ps, and a slow one $\tau_{I,3} = 4.6$–6.3 ps. Considering only protic solvents, $\tau_{I,3}$ shows a slight increase with viscosity. Within the error bars, the shortest two time constants and the corresponding DAS (≈610 nm) do not show a clear dependence on solvent properties. The DAS of $\tau_{I,3}$ shows 40 nm blueshift (640–620 nm) as we go to less polar solvents, both protic and nonprotic (Fig. 8, Table 1), but no trend shows up that includes all solvents. As the time-integrated fluorescence is mainly a time-average of the DAS of band I, they are expected to show the same solvent dependence. Indeed, for decreasing dielectric constant, all the DAS of band I gradually acquire larger spectral width and their maxima converge to the same wavelength (extreme case OctOH, Table 1).

Finally, comparing band II to the normalized bands I, it is found that band II loses weight in less polar solvents (Fig. 8). We observe 50% reduction going from MeOH to OctOH and 25% reduction from DCM to cHex.

In summary, we find that a), the peak-to-peak Stokes shifts of the PSBRs are very large (>6500 cm^{-1}) and are comparable, despite large differences in the solvent properties. This suggests that the Stokes shifts are dominated by intramolecular relaxation, even in polar solvents such as MeOH; b), the emission spectra observed at shortest delay time (within the excitation pulse width) are considerably Stokes shifted, suggesting a sub-50 fs energy relaxation process; c), the PSBR fluorescence is composed of two distinct fluorescence bands, a high-energy one decaying in a biexponential fashion in ≤30 fs and 150 ± 20 fs, and a low-energy one rising in 130 ± 30 fs, and decaying in a triexponential fashion with time constants of $\tau_{I,1} \approx 0.6$ ps, $\tau_{I,2} \approx 1.5$–2.5 ps, and $\tau_{I,3} \approx 4$–6 ps; and d), all reported timescales show no or only a mild dependence with either the solvent dielectric constant or viscosity.

DISCUSSION

Origin of the fluorescence bands

Before discussing the different relaxation times, we need to clarify the origin of the two fluorescence bands. The high-

energy band II is not due to unprotonated SBR molecules, as these are excited to a very small extent and have lifetimes of 30–50 ps (Bachilo et al., 1996). It is also not due to hot molecules in the S_1 excited state, as vibrational relaxation would lead to a wavelength-dependent decay time, gradually increasing with decreasing emission wavelength. In contrast, the SVD analysis shows that two decay times (Table 1) can be attributed to the entire band II. This behavior is independent of solvent, implying that the decay of band II is not due to an ultrafast dielectric response of the solvent (Horng et al., 1995). In addition, the data show a clear change of the fluorescence behavior in the intermediate region between band II and band I (Fig. 4). We therefore attribute bands I and II to the S_1–S_0 and S_2–S_0 transitions, respectively. Unlike for the electronic structure calculated for PSBR in gas phase (De Vico et al., 2002), solvent-induced mixing of the dipole-forbidden S_2 state with the dipole-allowed S_1 may take place and lead to excitation at 425 nm of the S_2 alongside the S_1 state.

The ultrafast dynamics (<200 fs)

Two ultrafast unresolved sub-50 fs components are observed: a), the shift of the emission away from the energy of excitation leading to a rise of band I and II, and b), the unresolved decay of band II ($\tau_{II,1}$). According to theory (González-Luque et al., 2000), the process behind (a) is most probably the relaxation along high-frequency skeletal modes, overdamped by anharmonic coupling to low-frequency modes, and expected to occur on a 20 fs timescale, as the first event associated with bond order change in S_1. As higher vibrational levels are populated with the excitation at 425 nm, this leads to a broad emission spectrum even before energy dissipation has taken place. Intramolecular vibrational energy redistribution (IVR) is then operative, reducing the high- and low-energy wing of the emission bands. This may be the origin for the fast sub-50 fs components in the decay of S_2 ($\tau_{II,1}$). Such ultrashort intramolecular vibrational energy redistribution times were reported for large molecules in condensed phase (Cerullo et al., 2001). The longer decay component of band II ($\tau_{II,2} = 140$–170 fs) is due to internal conversion from S_2 to S_1, as it reflects the rise of band I. The high relaxation rate may indicate a surface crossing (conical intersection) between both states.

Decay times of band II, stationary points, and isomerization paths

For an interpretation of the slower decay times $\tau_{I,1}$–$\tau_{I,3}$ related to the decay of band I, the following points should be taken into consideration: 1), the above intramolecular relaxation processes populate the state from which fluorescence occurs. Loosening of the C=C double bonds leads to a possibility of populating different conformations. Upon photoexcitation, retinal is considered to become very flexible due to a loosening of all C=C bonds of the conjugate chain (Kobayashi et al., 2001). Experiments on all-*trans* retinal in solvents suggest that isomerization occurs after 1 ps only (Hamm et al., 1996; Kandori and Sasabe, 1993; Logunov et al., 1996). We therefore propose that the emission stems from different quasistationary states (called stationary points [SP]; González-Luque et al., 2000) on the S_1 potential surface, corresponding to different conformations of the chromophore, which will lead to the different isomers that are known to be formed in solutions; and 2), isomerization of all-*trans* PSBR has an overall efficiency of only 15%–22% in solutions (Becker and Freedman, 1985). In other words, most (>75%) of the excited molecules do not undergo isomerization and come back to the all-*trans* ground state.

The properties of the different SPs give rise to the distinct fluorescence decay times and DAS (Table 1, Figs. 6 *A* and 7 *A*). The amplitudes are a measure of the relative populations right after the initial ultrafast relaxation period (>150 fs). The decay constant $\tau_{I,1} = 0.5$–0.64 ps is observed in the individual decay kinetics for every solvent. In MeOH, the $\tau_{I,1}$ component is observed only at shorter wavelengths, whereas in cHex it is present throughout almost the entire wavelength range, in particular also in the low-energy wing (cf. Fig. 7 *A*). It does not show up as a rise time, in contrast to $\tau_{II,2}$. It is therefore not associated with cooling, as previously suggested (Hamm et al., 1996). Rather, we propose that $\tau_{I,1}$ is associated with a nonisomerizing path, i.e., internal back conversion (IBC), since most chromophores relax back to the all-*trans* ground state (Freedman and Becker, 1986). It is plausible to attribute the fastest decay rate to the most efficient process, as the relative populations of the SPs are being equilibrated due to vibrational energy relaxation on a ps timescale (Kovalenko et al., 2001). This equilibration thus represents a possible loss channel for the SP ($\tau_{I,1}$), which is in the end avoided due to the shortness of $\tau_{I,1}$. This assignment is corroborated by the observation that the amplitudes of $\tau_{I,1}$ are larger for less polar solvents, consistent with a decrease of the isomerization yield found in high pressure liquid chromatography (HPLC) experiments (Koyama et al., 1991).

$\tau_{I,2}$ and $\tau_{I,3}$ are almost identical to those found by other authors (Kandori and Sasabe, 1993; Hamm et al., 1996; Logunov et al., 1996), and we likewise attribute them to isomerization. We add here the fact that the DAS are displaced in energy and are somewhat solvent dependent (Figs. 6 *A* and 7 *A*), which suggests that these decay times are related to the formation of different *cis*-isomers. The faster $\tau_{I,2}$ may lead to the preferentially formed 11-*cis* isomer, whereas the slower $\tau_{I,3}$ with smaller amplitude may represent the other isomerization channels (Becker and Freedman, 1985). The amplitudes of these decay times do not represent the fractions of isomerized to all-*trans* molecules determined in a HPLC analysis (Freedman and Becker, 1986; Koyama et al., 1991). This may be due to additional branching

between *cis* formation and return to the all-*trans* ground state, which occurs after depopulation of the SPs, at the conical intersections with S_0 for large torsional angles (De Vico et al., 2002). Moreover, secondary ground state isomerization processes, which occur at longer times and are not spectroscopically detectable, may also contribute to the isomer ratio determined by HPLC.

Influence of solvent properties

In general, the decay constants show hardly any dependence on dielectric constant, viscosity, or density of the solvents. This is also the case for the average fluorescence lifetime $\langle\tau\rangle = \sum_{i=1}^{3} a_{I,i}\tau_{I,i}$ (Table 1).

The exception being $\tau_{I,3}$, which shows an increase by $<70\%$ with viscosity, this only in protic solvents and even though the viscosity increases 15-fold (Table 1). A similar behavior has recently been reported for the different chromophore forms of the green fluorescent protein in solutions (Litvinenko et al., 2003). It points to a ''volume-conserving'' isomerization process (''hula twist'' (Liu and Asato, 1985) or ''bicycle pedal'' (Warshel, 1976)).

Alternative explanations for biexponential isomerization dynamics ($\tau_{I,2}$ and $\tau_{I,3}$) have been proposed in the literature. Inhomogeneities in the solvent environment may lead to different isomerization times and explain the different decay times (Vengris et al., 2004). OctOH is known to be a complex-associated solvent (Czarnecki and Orzechowski, 2003), which could indeed present this effect. However, the values of $\tau_{I,2}$ and $\tau_{I,3}$ and their amplitudes do not differ very much for the various solvents. Alternatively, the presence of a barrier along the *trans-cis* isomerization path can also lead to a biexponential decay (Logunov et al., 1996), in combination with a nonthermal distribution near the SP (Hamm et al., 1996; Kandori and Sasabe, 1993; Logunov et al., 1996). The fact that the DAS of $\tau_{I,2}$ and $\tau_{I,3}$ are different speaks against the isomerization barrier model. The solvent dependence of these DAS rather suggests that they come from different SPs with solvent-dependent potential energies.

Calculations for a PSBR analog in vacuum have shown that, when the molecule evolves along the torsional mode, the transition dipole moment decreases (Cembran et al., 2003), leading to quenching of fluorescence before the conical intersection is reached. This implies that the fluorescence reflects only the residence time in the ''optically active window'' of the SP (Kandori and Sasabe, 1993). This may be the reason why the excited state lifetimes of locked PSBR analogs in solution are very similar to that of free all-*trans* PSBRs (Hou et al., 2001). Likewise, there is no spectral red-shift associated with the torsional motion on the timescales of $\tau_{I,2}$ and $\tau_{I,3}$. This situation rather suggests that the fluorescence spectrum is an ensemble average over molecules with different degrees of torsion.

Comparison with bacteriorhodopsin

The lack of a clear cut dependence of the timescales with solvent properties suggests that the dynamics in solvents is governed by intramolecular mechanisms, in line with the comparable Stokes shifts found in the steady-state spectra for both protic and nonprotic solvents. For all solvents studied, the peak-to-peak Stokes shift is ~40%–50% larger than for bR (Haacke et al., 2001; Kennis et al., 2002), even in cHex (Table 1). It is dominated by intramolecular relaxation, and is 3 times larger than the intramolecular part of the Stokes shift in bR (1500–2000 cm^{-1}; Kennis et al., 2002; Loppnow et al., 1992). This directly suggests that the PSBRs in solvents are free to undergo structural relaxation of larger amplitudes than in the tight protein binding cavity.

In the protein, isomerization of retinal is known to occur without dramatic structural changes (Schobert et al., 2002). If we consider the above interpretation of the fluorescence decay times, we can conclude that in solvents these mild structural changes will not be strongly affected by the environment as the solvent cages are large enough to allow any small amplitude motion of retinal. Given that the backbone is loosened as a result of excitation, isomerization takes place around several C=C bonds, and all selectivity is lost. The lack of a dependence of the solvent dielectric constant also hints at a minor role played by electrostatic interactions. In the protein, the environment is tighter and the steric effects force the system to undergo isomerization preferentially around C13. In addition, the protein inhibits IBC. Experimental work on bR reconstituted with non-isomerizing retinal analogs indicated a lifetime of 18–19 ps for this process (Delaney et al., 1995; Ye et al., 1999; Haacke et al., 2001), in contrast to the sub-ps $\tau_{I,1}$ we observe here. It appears that the bond selectivity for isomerization controlled by the protein environment is possibly imposed during the entire excited state relaxation: steering vibrational relaxation preferentially into reactive SPs, and inhibiting IBC from the nonreactive SPs.

CONCLUSIONS

We have studied the ultrafast photophysics of all-*trans* PSBR in different protic and aprotic solvents. Steady-state spectra indicate large differences with respect to PSBR in the protein binding pocket, in particular a very large (~6500 cm^{-1}) intramolecular contribution to the Stokes shift. The time- and wavelength-resolved fluorescence up-conversion data reveal contributions of two electronic states, S_2 and S_1, to the sub-200 fs emission. In addition, different excited state relaxation processes are identified. A first sub-50 fs skeletal stretch relaxation causes the time-zero spectra to be Stokes-shifted by ~6000 cm^{-1}, with respect to absorption. Intramolecular energy relaxation is operative on a 50–150 fs timescale. Along with the direct excitation of S_1, it populates different fluorescent states that decay with three distinct

lifetimes. A 0.50–0.65 ps solvent-independent fluorescence decay component is interpreted as the all-*trans* ground state recovery, in line with the small isomerization yield of retinal in solvents. Two ps-long decay components are related to the torsional motion leading to the conical intersections for isomerization. No clear cut dependence on dielectric constant, viscosity, or density of the solvents has been identified, suggesting that most of the ultrafast dynamics presented here are dominated by intramolecular processes, probably due to the mild structural changes of retinal upon isomerization, which is not affected by the ''loose'' solvent cage. On the other hand, for the protein, we suggest that the significantly more steric environment causes the selective isomerization around the C13 atom. In addition, the ''catalytic'' action of the protein for an increased isomerization yield seems to imply the inhibition of IBC on the path from the FC region to the conical intersection. Finally, solvents seem to modulate the electronic structure, leading to spectral shifts of band I and II and to changes in the DAS.

The authors thank S. Ruhman, S. Schenkl, and F. van Mourik for valuable comments and suggestions. We are grateful to M. Olivucci and M. Garavelli for sharing unpublished results.

Financial support was provided by the Swiss National Science Foundation (FNRS) within the National Centre of Competence in Research ''Quantum Photonics'', the project grant 2153-065135, and the ''PROFIL-2'' grant for S.H. Further funding is kindly acknowledged from the ''Fondation Herbette'' of the University of Lausanne, Switzerland, where this work was initiated.

REFERENCES

Bachilo, S. M., S. L. Bondarev, and T. Gillbro. 1996. Fluorescence properties of protonated and unprotonated Schiff bases of retinal at room temperature. *J. Photochem. Photobiol. B: Biol.* 34:39–46.

Bachilo, S. M., and T. Gillbro. 1999. Fluorescence of retinal Schiff base in alcohols. *J. Phys. Chem. A.* 103:2481–2488.

Becker, R. S., and K. Freedman. 1985. A comprehensive investigation of the mechanism and photophysics of isomerization of a protonated and unprotonated Schiff base of *11-cis* retinal. *J. Am. Chem. Soc.* 107:1477–1485.

Birge, R. B., and C.-F. Zhang. 1990. Two-photon double resonance spectroscopy of bacteriorhodopsin. Assignment of the electronic and dipolar properties of the low-lying 1A-like and 1B-like states. *J. Chem. Phys.* 92:7178–7195.

Cembran, A., F. Bernardi, M. Olivucci, and M. Garavelli. 2003. Excited state singlet manifold and oscillators features of a nonatetraeniminium retinal chromophore model. *J. Am. Chem. Soc.* 125:12509–12519.

Cerullo, G., G. Lanzani, M. Zavelani-Rossi, and S. De Silvestri. 2001. Early events of energy relaxation in all-*trans* β-carotene following sub-10 fs optical-pulse excitation. *Phys. Rev. B.* 63:241104.

Czarnecki, M. A., and K. Orzechowski. 2003. Effect of temperature and concentration on self-association of Octan-3-ol studied by vibrational spectroscopy and dielectric measurements. *J. Phys. Chem. A.* 107:1119–1126.

De Vico, L., C. S. Page, M. Garavelli, F. Bernardi, R. Basosi, and M. Olivucci. 2002. Reaction path analysis of the ''tunable'' photoisomerization selectivity of free and locked retinal chromophores. *J. Am. Chem. Soc.* 124:4124–4134.

Delaney, J. K., T. L. Brack, G. H. Atkinson, M. Ottolenghi, G. Steinberg, and M. Sheves. 1995. Primary picosecond molecular events in the photoreaction of the bR5.12 artificial bacteriorhodopsin pigment. *Proc. Natl. Acad. Sci. USA.* 92:2101–2105.

Dexheimer, S. L., Q. Wang, L. A. Peteanu, W. T. Pollard, R. A. Mathies, and C. V. Shank. 1992. Femtosecond impulsive excitation of non-stationary vibrational states in bacteriorhodopsin. *Chem. Phys. Lett.* 188:61–66.

Dobler, J., W. Zinth, W. Kaiser, and D. Oesterhelt. 1988. Excited-state reaction dynamics of bacteriorhodopsin studied by femtosecond spectroscopy. *Chem. Phys. Lett.* 144:215–220.

Du, M., and G. R. Fleming. 1993. Femtosecond time-resolved fluorescence spectroscopy of bacteriorhodopsin: direct observation of excited state dynamics in the primary step of the proton pump cycle. *Biophys. Chem.* 48:101–111.

Freedman, K. A., and R. S. Becker. 1986. Comparative investigation of the photoisomerization of the protonated and unprotonated *n*-butylamine Schiff bases of *9-cis, 11-cis, 13-cis* and *all-trans*-retinals. *J. Am. Chem. Soc.* 108:1245–1251.

González-Luque, R., M. Garavelli, F. Bernardi, M. Merchán, M. A. Robb, and M. Olivucci. 2000. Computational evidence in favor of a two-state, two-mode model of the retinal chromophore isomerization. *Proc. Nat. Acad. Sci.USA.* 97:9379–9384.

Haacke, S., R. A. Taylor, I. Bar-Joseph, M. J. S. P. Brasil, M. Hartig, and B. Deveaud. 1998. Improving the signal-to-noise ratio of femtosecond luminescence up-conversion by multichannel detection. *JOSA B.* 15: 1410–1417.

Haacke, S., S. Vinzani, S. Schenkl, and M. Chergui. 2001. Spectral and kinetic fluorescence properties of native and non-isomerizing retinal in bacteriorhodopsin. *ChemPhysChem.* 2:310–315.

Hamm, P., M. Zurek, T. Röschinger, H. Patzelt, D. Oesterhelt, and W. Zinth. 1996. Femtosecond spectroscopy of the photoisomerization of the protonated Schiff base of all-*trans* retinal. *Chem. Phys. Lett.* 263:613–621.

Herbst, J., K. Heyne, and R. Diller. 2002. Femtosecond infrared spectroscopy of bacteriorhodopsin chromophore isomerization. *Science.* 297:822–825.

Heyne, K., J. Herbst, B. Dominguez-Herradon, U. Alexiev, and R. Diller. 2000. Reaction control in bacteriorhodopsin: impact of Arg82 and Asp85 on the fast retinal isomerization. *J. Phys. Chem.* 104:6053–6058.

Horng, M. L., J. A. Gardecki, A. Papazyan, and M. Maroncelli. 1995. Subpicosecond measurements of polar solvation dynamics: coumarin 153 revisited. *J. Phys. Chem.* 99:17311–17337.

Hou, B., N. Friedman, S. Ruhman, M. Sheves, and M. Ottolenghi. 2001. Ultrafast spectroscopy of the protonated Schiff bases of free and C13 = C14 locked retinals. *J. Phys. Chem. B.* 105:7042–7048.

Huang, J., Z. Chen, and A. Lewis. 1989. Second-harmonic generation in purple membrane-poly(vinyl alcohol) films: probing the dipolar characteristics of the bacteriorhodopsin chromophore in bR570 and M410. *J. Phys. Chem.* 93:3314–3320.

Huppert, D., and P. M. Rentzepis. 1986. Time-resolved luminescence study of protonated Schiff bases. *J. Phys. Chem.* 90:2813–2816.

Kandori, H., and H. Sasabe. 1993. Excited-state dynamics of a protonated Schiff base of all-*trans* retinal in methanol probed by femtosecond fluorescence measurement. *Chem. Phys. Lett.* 216:126–132.

Kennis, J. T. M., D. S. Larsen, K. Ohta, M. Facciotti, R. M. Glaeser, and G. R. Fleming. 2002. Ultrafast protein dynamics of bacteriorhodopsin probed by photon echo and transient absorption spectroscopy. *J. Phys. Chem. B.* 106:6067–6080.

Kobayashi, T., T. Saito, and H. Ohtani. 2001. Real-time spectroscopy of transition states in bacteriorhodopsin during retinal isomerization. *Nature.* 414:531–534.

Kovalenko, S. A., R. Schanz, H. Hennig, and N. P. Ernsting. 2001. Cooling dynamics of an optically excited molecular probe in solution from femtosecond broadband transient absorption spectroscopy. *J. Chem. Phys.* 115:3256–3273.

Koyama, Y., K. Kubo, M. Komori, H. Yasuda, and Y. Mukai. 1991. Effect of protonation on the isomerization properties of *n*-butylamine Schiff base of isomeric retinal as revealed by direct HPLC analyses. *Photochem. Photobiol.* 54:433–443.

Lakowicz, J. R. 1999. Principles of Fluorescence Spectroscopy. Kluwer Academic/Plenum Publishers, New York.

Litvinenko, K. L., N. M. Webber, and S. R. Meech. 2003. Internal conversion in the chromophore of the green fluorescent protein: temperature dependence and isoviscosity analysis. *J. Phys. Chem. A.* 107:2616–2623.

Liu, R. S. H., and A. E. Asato. 1985. The primary process of vision and the structure of bathorhodopsin: a mechanism for photo-isomerization of polyenes. *Proc. Nat. Acad. Sci. USA.* 82:259–263.

Logunov, S. L., L. Song, and M. A. El-Sayed. 1996. Excited-state dynamics of a protonated retinal Schiff base in solution. *J. Phys. Chem.* 100:18586–18591.

Loppnow, G. R., R. A. Mathies, T. R. Middendorf, D. S. Gottfried, and S. G. Boxer. 1992. Photochemical hole-burning spectroscopy of bovine rhodopsin and bacteriorhodopsin. *J. Phys. Chem.* 96:737–745.

Maroncelli, M., and G. R. Fleming. 1988. Computer simulation of the dynamics of aqueous solvation. *J. Chem. Phys.* 89:5044–5069.

Mathies, R. A., C. H. Brito Cruz, W. T. Pollard, and C. V. Shank.1988. Direct observation of the femtosecond excited state *cis-trans* isomerization in bacteriorhodopsin. *Science.* 240:777–779.

Mathies, R. A., and L. Stryer. 1976. Retinal has a highly dipolar vertically excited singlet state: implications for vision. *Proc. Nat. Acad. Sci. USA.* 73:2169–2178.

Nonella, M. 2000. Electrostatic protein-chromophore interactions promote the all-*trans* → 13-*cis* isomerization of the protonated retinal Schiff base in bacteriorhodopsin: an ab initio CASSCF/MRCI study. *J. Phys. Chem. B.* 104:11379–11388.

Oesterhelt, D., and W. Stoeckenius. 1971. Rhodopsin-like protein from the purple membrane of Halobacterium halobium. *Nat. New Biol.* 233:149–152.

Polland, H. J., M. A. Franz, W. Zinth, W. Kaiser, E. Kölling, and D. Oesterhelt. 1986. Early picosecond events in the photocycle of bacteriorhodopsin. *Biophys. J.* 49:651–662.

Ponder, M., and R. A. Mathies. 1983. Excited-state polarizabilities and dipole moments of diphenylpolyenes and retinal. *J. Phys. Chem.* 87:5090–5098.

Reynolds, L., J. A. Gardecki, J. V. Frankland, M. L. Horng, and M. Marconcelli. 1996. Dipole solvation in nonpolar solvents: experimental studies of reorganization energies and solvation dynamics. *J. Phys. Chem.* 100:10337–10354.

Riddick, J. A., W. B. Bunger, and T. K. Sakano. 1986. Organic Solvents. Wiley, New York.

Schobert, B., J. Cupp-Vickery, V. Hornak, S. O. Smith, and J. K. Lanyi. 2002. Crystallographic structure of the K intermediate of bacteriorhodopsin: conservation of free energy after photoisomerization of the retinal. *J. Mol. Biol.* 321:715–726.

Schoenlein, R. W., L. A. Peteanu, R. A. Mathies, and C. V. Shank. 1991. The first step in vision: femtosecond isomerization of rhodopsin. *Science.* 254:412–415.

Sharkov, A. V., A. V. Pakulev, S. V. Chekalin, and Y. A. Matveetz. 1985. Primary events in bacteriorhodopsin probed by subpicosecond spectroscopy. *Biochim. Biophys. Acta.* 808:94–101.

Song, L., and M. A. El-Sayed. 1998. Primary step in bacteriorhodopsin photosynthesis: bond stretch rather than angle twist of its retinal excited-state structure. *J. Am. Chem. Soc.* 120:8889–8890.

Song, L., M. A. El-Sayed, and J. K. Lanyi. 1993. Protein catalysis of the retinal subpicosecond photoisomerization in the primary process of bacteriorhodopsin photosynthesis. *Science.* 261:891–894.

Vengris, M., M. A. van der Horst, G. Zgrablic, I. H. M. van Stokkum, S. Haacke, M. Chergui, K. J. Hellingwerf, R. van Grondelle, and D. S. Larsen. 2004. Contrasting the excited-state dynamics of the photoactive yellow protein chromophore: protein versus solvent environments. *Biophys. J.* 87:1848–1857.

Wang, Q., R. W. Schoenlein, L. A. Peteanu, R. A. Mathies, and C. V. Shank. 1994. Vibrationally coherent photochemistry in the femtosecond primary event of vision. *Science.* 266:422–424.

Warshel, A. 1976. Bicycle-pedal model for the first step in the vision process. *Nature.* 260:679–683.

Xu, D., C. Martin, and K. Schulten. 1996. Molecular dynamics study of early picosecond events in the bacteriorhodopsin photocycle: dielectric response, vibrational cooling and the J,K intermediates. *Biophys. J.* 70:453–460.

Ye, T., N. Friedman, Y. Gat, G. H. Atkinson, M. Sheves, M. Ottolenghi, and S. Ruhman. 1999. On the nature of the primary light-induced events in bacteriorhodopsin: ultrafast spectroscopy of native and $C_{13} = C_{14}$ locked pigments. *J. Phys. Chem. B.* 103:5122–5130.

Zgrablić, G., K. Voïtchovsky, M. Kindermann, M. Chergui, and S. Haacke.2004. Ultrafast photophysics of the protonated Schiff base of retinal in alcohols studied by femtosecond fluorescence up-conversion. *In* Femtochemistry and Femtobiology: Ultrafast Events in Molecular Science. M. Martin and J. T. Hynes, editors. Elsevier, Paris.